AIAA

A02-13923

AIAA2002-0793

Laser Diagnostics of Atomic Oxygen in Arc-Heater Plumes

M. Matsui, K. Komurasaki, Y. Arakawa

University of Tokyo, Tokyo, Japan

41th Aerospace Sciences Meeting and Exhibit

14-17 January 2002

Reno. Nevada

Laser Diagnostics of Atomic Oxygen in Arc-Heater Plumes

Makoto MATSUI*, Kimiya KOMURASAKI[†], and Yoshihiro ARAKAWA[‡]

University of Tokyo, Hongo 7-3-1, Bunkyo, Tokyo 113-0033, Japan

Abstract

Laser absorption spectroscopy has been conducted to measure chemical compositions of high enthalpy flows generated by constrictor type arc-heaters. Distributions of metastable atomic oxygen and argon number density and translational temperature were obtained from absorption profiles at 777.19nm and 840.82nm. As a result, it was found that the density peak of atomic oxygen has a peak off-axis in the vicinity of the nozzle exit, and the peak moves toward the centerline in the downstream. Therefore, oxygen injected at the constrictor is not thought to be enough mixed with argon in the nozzle and then diffuse from outside toward the centerline, being dissociated in the plume out of the nozzle. Translational temperature deduced from OI 777.19nm absorption line was higher than that from ArI 840.82nm.

Introduction

Arc-heaters are used for the tests of Thermal Protection Systems for reentry vehicles. However, exact plume conditions are mostly unknown because it is usually in thermo-chemical nonequilibrium. Therefore, measurements of chemical composition in the plume will provide useful information for TPS researches, and for validation of numerical codes for high-speed reacting gas flow simulation.

In TPS tests, two kinds of arc-heaters are often used. One is a constrictor type [1,2] and the other is a segmented cathode type. [3,4] The schematic of both types are shown in Fig.1. The advantage of segmented cathode type arc-heaters is their high input power. Since the input power is determined by a throat or a constrictor radius, their input power can be three orders magnitude higher than that of the constrictor type arc-heaters. In addition, air can be used as a working gas. As for the constrictor type arc-heaters, the advantages are simple structure, easy maintenance, and long operational time. Due to these operational conveniences, constrictor arc-heaters are widely used for material tests. However, to prevent the cathode from oxidization, nitrogen-oxygen gas is used to simulate airflow and oxygen is injected at the constrictor part.

Number density of atomic oxygen in a plume is quite important for studies on surface catalysis and oxidization of TPS. Therefore, the absorption spectroscopy has been conducted targeting the atomic oxygen in a plume.

In our previous research, [5] distributions of atomic oxygen in a shock layer formed in front of a TPS material was measured in a nitrogen-oxygen flow. As a result, the peak of the density profile was located off-axis as shown in Fig.2.

This result gave us a following picture of the mixing process of nitrogen and oxygen as shown in Fig.3 Oxygen injected at the constrictor is not enough mixed with nitrogen in the nozzle. Then, oxygen diffuses from outside toward the centerline, being dissociated in the plume out of the nozzle. Since, oxygen does not pass through the high temperature cathode-jet region, degree of dissociation is unexpectedly small.

To clarify this hypothesis, it is necessary to obtain number density distributions of atomic oxygen in the free stream. However, absorption was too weak to detect in a nitrogen-oxygen free stream.

Therefore, in this research, absorption measurement was conducted on an argon-oxygen free stream. In the argon-oxygen flow, the following collisions take place. [6]

$$O_2 + Ar^* \rightarrow O\,(2p^{4\,3}P) + O\,(2p^{4\,1}S \text{ or } 2p^{4\,1}D) + Ar$$
$$O\,(2p^{4\,3}P) + Ar^* \rightarrow O^*\,(3p^{3}P) + Ar$$
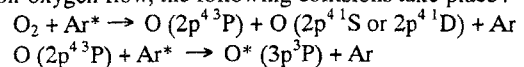
Here, Ar* is metastable argon and Ar is ground state argon. Owing to these collisions, the number density of metastable oxygen $(3p^5S)$ is quite larger than that in the nitrogen-oxygen flow. Therefore, the absorption in the argon-oxygen flow is enough strong to detect.

The absorption profile is obtained by modulating the laser wavelength around the absorption line. Number density in a metastable state is deduced from its integrated absorption coefficient and translational temperature is from its broadening width.

* Graduate student, Department of Advanced Energy, Student Member AIAA, matsui@al.t.u-tokyo.ac.jp

[†] Associate Professor, Department of Advanced Energy, Member AIAA,

[‡] Professor, Department of Aeronautics and Astronautics, Member AIAA

Measurement Method

Recently, non-intrusive spectroscopy, especially emission one is actively done to examine the characteristic of such high temperature and high Mach number flows. [7,8]

Laser Induced Fluorescence is one of the most powerful spectroscopy because it is able to get the atomic number density of the ground state directly. In addition, this method is sensitive and applicable to a low-density flow ($\sim 10^8[\text{m}^{-3}]$). [9,10] However, it is not applicable to optically thick plasma due to strong spontaneous emission and reabsorption. Moreover, a huge, expensive laser such as excimers is needed to excite the ground state of atoms.

Diode-laser absorption spectroscopy has two major advantages. It is applicable even to optically thick flows and it does not require the absolute absorption quantity but the relative absorption one, that is, the fractional absorption.

Absorption coefficient

The relationship between laser intensity I_ν and absorption coefficient k_ν in a substance is expressed by Beer-Lambert law as,

$$\frac{dI_\nu}{dx} = -k_\nu I_\nu \tag{1}$$

Equation (1) is integrated as,

$$\ln \frac{I_\nu}{I_{\nu 0}} = -\int k_\nu dx \tag{2}$$

Here, $I_{\nu 0}$ I_ν, ν are incident laser intensity, transmitted laser intensity, and laser frequency, respectively. Assuming axisymmetric distribution, the local absorption coefficient is obtained by the Abel inversion. [11]

Since the local absorption coefficient is a sum of absorption coefficient and a stimulated emission coefficient, the relationship between integrated absorption coefficient $K(r)$ and population density at the absorbing state n_i is given as [12,13]

$$K(r) = \int k_\nu d\nu = \frac{\lambda^2}{8\pi} \frac{g_j}{g_i} A_{ji} n_i \left[1 - \exp\left(-\frac{\Delta E_{ij}}{kT_{ex}}\right)\right] \tag{3}$$

Here, i, j are lower and upper energy levels, A_{ji} is the Einstein's emission coefficient, g_i and g_j are statistical weights, E, k and T_{ex} are energy level, Boltzmann constant and electronic excitation temperature, respectively. The transition data of atomic oxygen at 777.19nm and of argon at 840.82nm are shown in Table 1.

Table 1 Transition data

	i	j	λ(nm)	E_i(eV)	E_j(eV)	g_i	g_j	$A_{ji}(10^8\text{s}^{-1})$
OI	$3s^5S$	$3p^5P$	777.19	9.14	10.7	5	7	0.369
ArI	$4s^2[1/2]$	$4p^2[3/2]$	840.82	11.8	13.3	3	5	0.223

At 777.19 nm and 840.82nm, $\Delta E_{ij}/k$ are 18,500 K, and 17,100K, respectively. If $T_{ex} < \Delta E_{ij}/k$, stimulated emission is neglected and Eq. (3) is simplified as

$$K = \frac{\lambda^2}{8\pi} \frac{g_j}{g_i} A_{ji} n_i \tag{4}$$

Absorption profile

Absorption profile is broadened by various physical mechanisms, and is expressed by a convolution of the Lorentz-type and the Gauss-type distribution.

Doppler broadening

Doppler broadening is the statistical one originating from thermal motion of the particle. The profile is Gauss type and the full width at the half maximum $\Delta\nu_D$ is expressed as,

$$\Delta\nu_D = \frac{\sqrt{8R\ln 2}}{\lambda_0} \sqrt{\frac{T}{M}} \tag{5}$$

Here, c is the velocity of light, R is gas constant, λ_0 is the center frequency of the absorption, M is the atomic weight of the absorbing atom and T is the translational temperature.

Other broadenings

Natural broadening is caused by the fact that there is finite time for the transition, and its width is expressed as,

$$\Delta\nu = \frac{A_{ij}}{2\pi} \tag{6}$$

Pressure broadening is caused by collisions between atoms and particles around them and expressed as,

$$\Delta\nu_L = 1.95 \times 10^{13} p\sigma_L^2 \sqrt{\frac{2R}{\pi T}\left(\frac{1}{M_1} - \frac{1}{M_2}\right)} \tag{7}$$

Here, σ_L is effective collisional cross-section, p is the gas pressure, M_1 is atomic weight of absorbing atom, and M_2 is atomic weight of ambient gas.

Stark broadening originates from the fact that the degeneracy is solved by the electric field which a surrounding electron makes, and is expressed by as,[14]

$$\Delta\nu_s = 1.0 \times \left[1 + 1.75 \times 10^{-4} n_e^{1/4} \alpha \left(1 - 0.068 n_e^{1/6} T_e^{-1/2}\right)\right] n_e w \cdot 10^5 \tag{8}$$

Here, w is electron impact parameter, α is ion broadening parameter, n_e is electron density, and T_e is electron temperature. These three broadenings are all Lorenz type and three orders of magnitude smaller than that of Doppler broadening under our measurement conditions. Therefore, they are neglected. The relationship between these physical parameters and absorption profiles are illustrated in Fig.4.

Experimental Apparatus

Optical system

Figure 5 shows the schematic of an optical system used in this research. Tunable diode-lasers with an external cavity (Velocity Model 6300, New Focus, and DMD845, EOSI) were used as the laser oscillator. The line width of the both lasers is smaller than 300kHz. The modulation frequency and width were 10 Hz and 20 GHz, respectively. The optical isolator is used to prevent the reflected laser

beam from returning into the external cavity. The laser beam is divided into three beams by beam splitters. The first beam is directly detected by the photo-detector as a reference signal. The second is detected by a Fabry-perot, ethalon, whose free spectral range is 1 GHz. The third is lead to the chamber window through a multimode optical fiber. The fiber output is mounted on a one-dimensional traverse stage to scan the plume in radial directions. At the other side window, a parabola mirror is set and the laser beam can be detected without synchronizing the detector position with the laser scan. Spatial resolution is about 1mm.

JUTEM's Arc heater

The schematic of the arc-heater developed in the Japan Ultra-high Temperature Materials Research Center (JUTEM) is shown in Fig.6. Oxygen is injected at the constrictor part as described above. Diameter of constrictor is 4 mm. The flow Mach number is designed at 3. A photograph of the arc-heater plume is shown in Fig.7.

University of Tokyo's Arc-heater

The measurement was also conducted using the University of Tokyo's arc-heater. The schematic of the arc-heater is shown in Fig.8. The oxygen injection is the same as that of the JUTEM's arc-heater. Diameter of constrictor is 2 mm. The flow Mach number is designed at 2. The thermal efficiency was estimated about 60% from the increase in temperature of cooling water. A photograph of the arc-heater plume is shown in Fig.9.

Test conditions

Three cases were tested and the experimental conditions are listed in Table 2. Case #1 is the measurement of the distributions of metastable oxygen number density and the translational temperature using the OI 777.19nm absorption line in the argon-oxygen free stream generated by the JUTEM's arc-heater. The flow consists of 20 [slm] argon and 5 [slm] oxygen. The input power is 7.2 [kW] and specific enthalpy is about 6.1 [MJ/kg] assuming that thermal efficiency is 60%. The backpressure was kept at 38 [Pa].

Case #2 is the measurement using University of Tokyo's arcjet. The target line is also OI 777.19nm. The flow consists of 6 [slm] argon and 1.5 [slm] oxygen. The input power is 1.2 [kW] and specific enthalpy is 3.3 [MJ/kg]. The backpressure was kept at 26 [Pa].

Case #3 is the measurement of the metastable argon number density and the translational temperature using the ArI 840.82nm absorption line. The operating conditions are the same as Case #2.

Table 2 Experimental conditions

No	Gas flow	Specific Enthalpy	Target	Arc Generator
1	Ar: 20[slm] O_2: 5[slm]	6.1 [MJ/kg]	O I (777.19nm)	JUTEM arc-heater
2	Ar: 6[slm] O_2: 1.5[slm]	3.3 [MJ/kg]	O I (777.19nm)	University of Tokyo arc-heater
3	Ar: 6[slm] O_2: 1.5[slm]	3.3 [MJ/kg]	Ar I (840.82nm)	University of Tokyo arc-heater

Typical signals and a normalized absorption profile of metastable oxygen are shown in Figs. 10 and 11.

Experimental Result

Case #1

Figures 12 and 13 show the distributions of metastable oxygen number density and the translational temperature, respectively. At z=100mm, the number density profile has two peaks at r=20mm (z and r are defined by cylindrical coordinate and origin is taken at the center of nozzle exit). Then, these two peaks approach to the centerline in the downstream of the plume and combine at z=250mm. In contrast, the distribution of translational temperature at z=100mm has a peak on the centerline, and it separates into two peaks at z=150mm. The maximum number density and translational temperature are $3.1 \times 10^{16} \text{m}^{-3}$ and 6200K, respectively.

Case #2

Figures 14 and 15 show the distributions of metastable oxygen number density and translational temperature, respectively. The profile of number density distribution is similar to that of Case #1. That is, at z=0mm, the number density profile has two peaks at r=11mm. Then, these peaks approach to the centerline in the downstream of the plume and combine at z=60mm. The maximum number density is $3.5 \times 10^{16} \text{m}^{-3}$. Translational temperature is in the rage of 3600K ~ 4000K.

Case #3

Figures 16 and 17 show the distributions of metastable argon number density and translational temperature, respectively. Number density decreases monotonously along the centerline. The maximum number density and translational temperature are $3.0 \times 10^{17} \text{m}^{-3}$ and 2700K, respectively.

Discussion

Density distributions

The density peaks of metastable atomic oxygen were located off-axis at the nozzle exit and approached to the centerline in Cases #1 and #2 as shown in Figs 12 and 14. Although the profile of ground state is thought to be somehow different from that of metastable state, this result would support the hypothesis described above.

In Case #2, two density peaks located off-axis combine earlier than in Case #1. This is partly because the size of the University of Tokyo's arc-heater is smaller than JUTEM's and the shear in the free jet is stronger resulting in larger turbulent transport, and partly because the flow Mach number of former plume is smaller than the latter one.

In the downstream, number density of metastable atomic oxygen is increasing, while that of metastable argon

3
Institute of Aeronautics and Astronautics

is decreasing as shown in Figs. 14 and 16. This is because oxygen is being dissociated in the plume, and metastable argon is being deexcited by collision and radiation.

Translational Temperatures

Translational temperature deduced from the OI 777.19nm absorption line was higher than that from the ArI 840.82nm absorption line as shown in Figs. 15 and 17.It is difficult to assume that two translational temperatures are different for different species because the translational relaxation time is much shorter than the flow time.

In argon-oxygen plasma, the following collisional process is known.

$$O\ (3p^3P) + Ar \rightarrow O\ (3p^5P) + Ar + \Delta E$$

Because the collision is accompanied by the release of 0.56 [eV] of translational energy, the assumption of a Doppler broadened emission line at the tranlational temperature cannot be considered valid. [15] This is thought to be one reason that translational temperature deduced from the OI 777.19nm absorption line is higher than that from the ArI 840.82nm absorption line. Therefore, the distribution of Fig.17 is thought to be more accurate for tranlational temperature measurement, it is better to use absorption lines except for OI 777.19nm.

Summary

Oxygen injected at the constrictor is not enough mixed with argon in the nozzle and then, diffuses from outside toward the centerline in the downstream.

Translational temperature deduced from OI 777.19nm absorption line becomes higher than actual. Therefore, other absorption line such as ArI 840.82nm should be used for the translational temperature.

Acknowledgment

References

[1] T. Laux, M. Feigl, M. Auweter-Kurtz and T. Stockle, Estimation of the Surface Catalycity of PVD-Coatings by Simultaneous Heat Flux and LIF Measurements in High Enthalpy Air Flows, AIAA Paper 2000-2364

[2] M. Ishii, M. Ito, K. Toki and K. Kuriki, Atomic oxygen flow facility using arcjet, International Symposium on Space Technology and Science, Vol.1 (1988), p363-368

[3] I. T. Salinas, C. Park, A.W. Strawa,N. Gopaul and J. S. Taunk, Spectral Measurements in the Arc Column of an Arc-Jet Wind Tunnel, AIAA Paper 94-2595

[4] M. Hinada, Y. Inatani, T. Yamada, and K. Hiraki, An Arc-Heated High Enthalpy Test Facility for Thermal Protection Studies, ISAS-RN-664

[5] Komurasaki, K, Sugimine, M, Hosoda, S., and Arakawa, Y.: Laser Absorption Measurement of Atomic Oxygen in Arc-Heater Plumes, AIAA Paper 2001-0814

[6] Minimo, M., Kimura, A., Nishida, M., Population and depopulation of O(3p5P) in a supersonic freejet of an O2-seeded Ar plasma, J. Chem. Phys., 72(1), 1980, p785-787

[7] H. Tahara, T. Taniguchi, K. Onoe and T. Yoshikawa, DC Arcjet Plasma characteristics using ammonia and mixture of nitrogen and hydrogen, AIAA Paper 99-3736, July, 1999

[8] Winter, M. W. and Auweter-Kurtz, M.: Boundary layer investigation in front of a blunt body in a subsonic air plasma flow by emission spectroscopic means, AIAA Paper 98-2460, June, 1998

[9] Storm, P. V. and Cappelli, M. A., Laser-induced fluorescence measurements within an arcjet thruser nozzle, AIAA Paper 95-2381, July 1995

[10] Feigl, M., Dennis, J. E., Fasoulas, S. and Auweter-Kurtz, M., Comparison of LIF and solid electrolyte sensor measurements of atomic and molecular oxygen in a plasma jet, AIAA paper 2000-0198, January 2000

[11] Deutch, M., Abel inversion with a simple analytic representation for experimental data, *Appl. Phys. Lett.*, Vol 42, pp 237-239, 1983

[12] Zel'dovich, Y. B., Raizer, Y. P., Hayes, W. D. and Probstain, R. F., *Physics of shock waves and high-temperature hydrodynamic phenomena*, Academic Press New York (1966), pp. 107-172

[13] Lochte-Holtgreven W., *Plasma Diagnostics*, Norty-Holland Publishing Company, Amsterdam (1968), pp. 9-65

[14] Arroyo, M. P., Langlogis, S. and Hanson, R. K., Diode-laser absorption technique for simultaneous measurement of multiple gasdynamic parameters in high-speed flows containing water vapor, *App. Opt.*, Vol. 33 (1994), pp.3296-3370

[15] Lawrence G. Piper, Electronic energy transfer between metastable argon and atoms and ground state oxygen atom, Chem. Phys. Vol 28, p276-279

[16] Griem, H., *Plasma Spectroscopy*, McGraw Hill, New York (1964)

[17] Herzberg, G., *Atomic spectra and atomic structure*, *Dover Publications*, New York (1944)
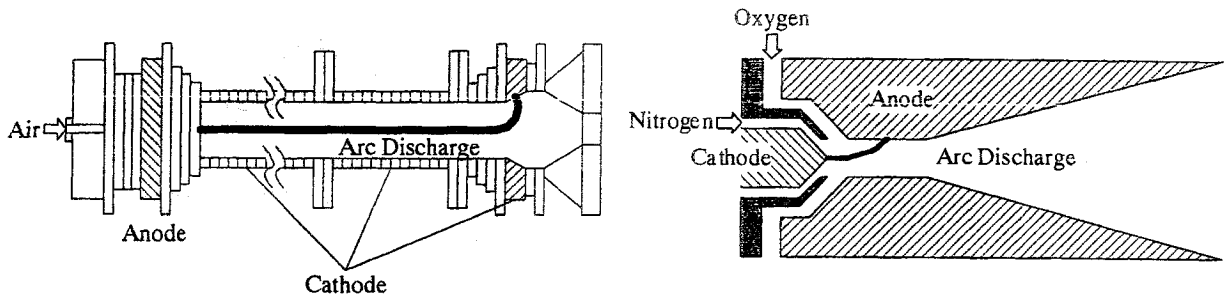
Fig.1 The schematic of segmented cathode type (left) and constrictor type (right) arc -heaters
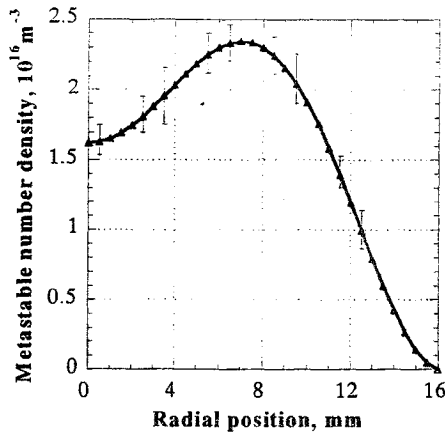
Fig.2 Radial distribution of metastable atomic oxygen number density in the shock layer
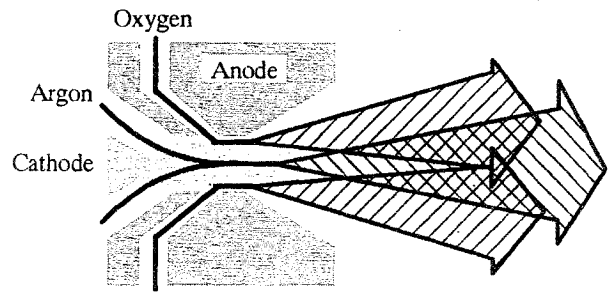
Fig.3 Mixing process
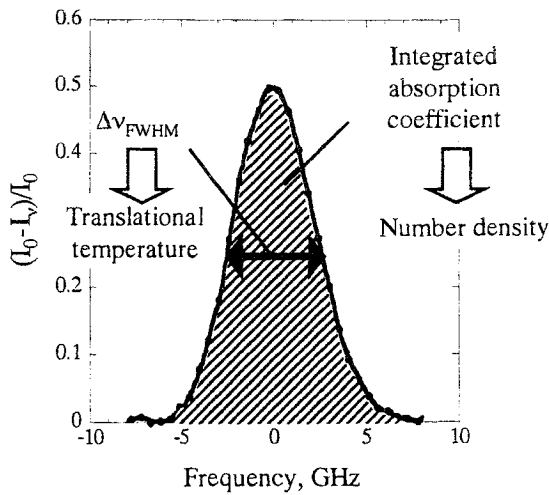
Fig.4 Relationship between physical properties and absorption profiles

Fig.5 Optical system

5
Institute of Aeronautics and Astronautics
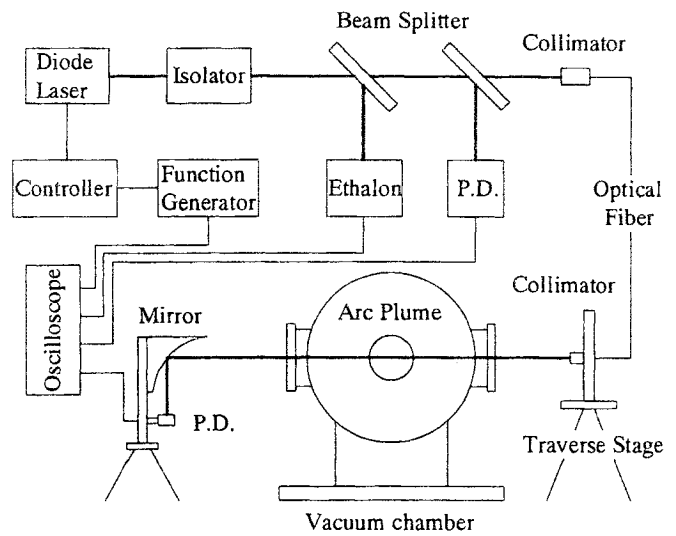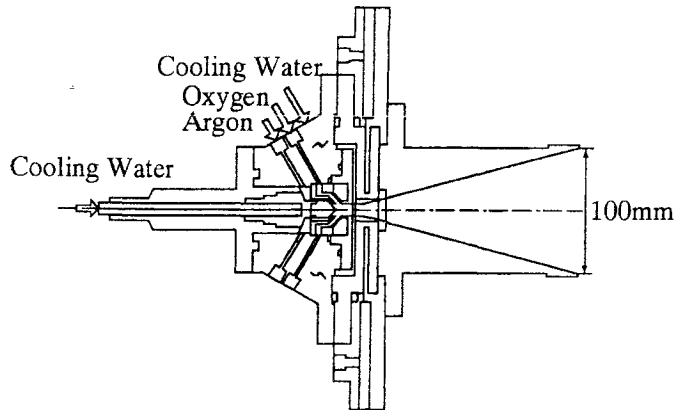
Fig.6 JUTEM's arc-heater
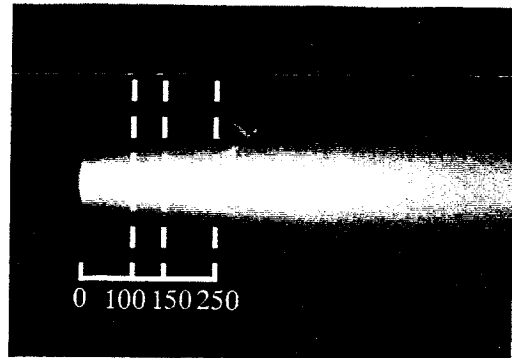
Fig.7 Argon-oxygen plume generated by JUTEM's arc-heater
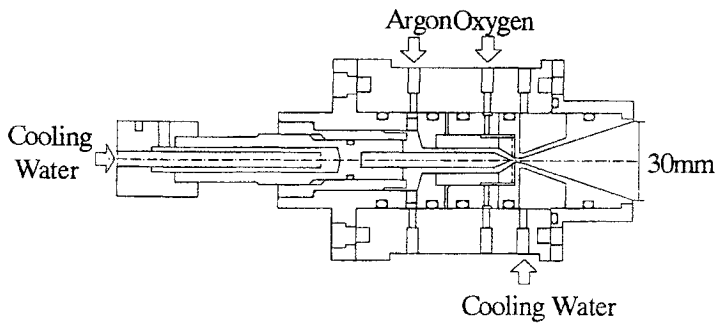
Fig.8 University of Tokyo's arc-heater
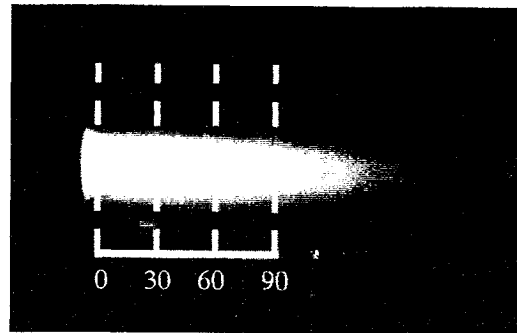
Fig.9 Argon-oxygen plume generated by university of Tokyo's arc-heater
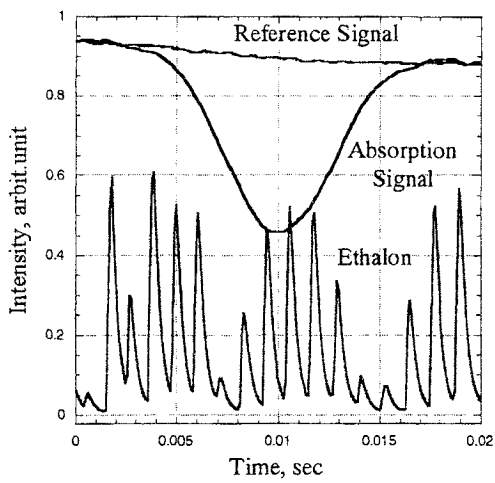
Fig.10 Typical signals

Fig.11 Normalized absorption profile

Institute of Aeronautics and Astronautics
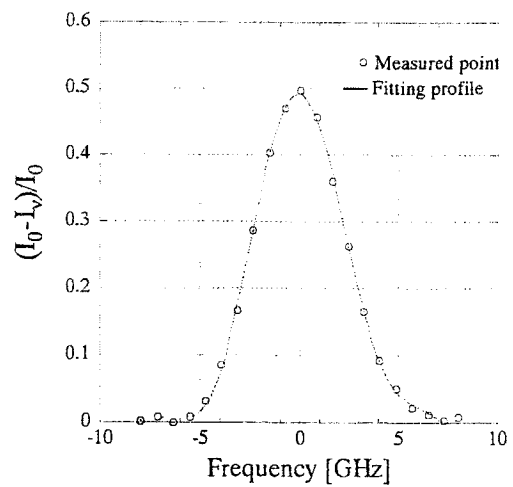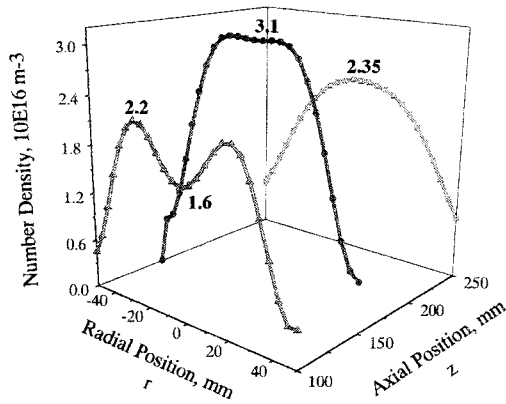
Fig.12 Number density of metastable oxygen in the argon-oxygen plume generated by JUTEM's arc-heater
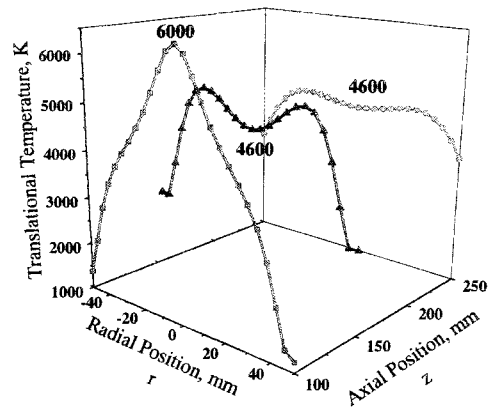
Fig.13 Translational temperature deduced from OI in the argon-oxygen plume generated by JUTEM's arc-heater
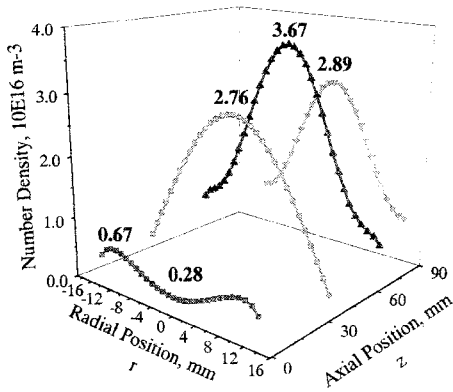
Fig.14 Number density of metastable oxygen in the argon-oxygen plume generated by University of Tokyo's arc-heater
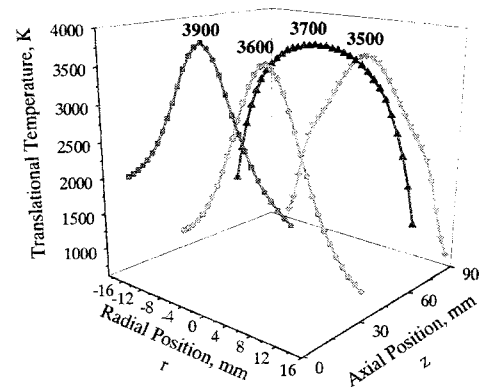
Fig.15 Translational temperature deduced from OI in the argon-oxygen plume generated by University of Tokyo's arc-heater
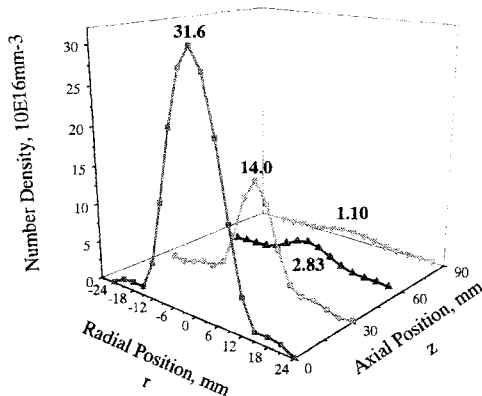
Fig.16 Number density of metastable oxygen in the argon-oxygen plume generated by University of Tokyo's arc-heater
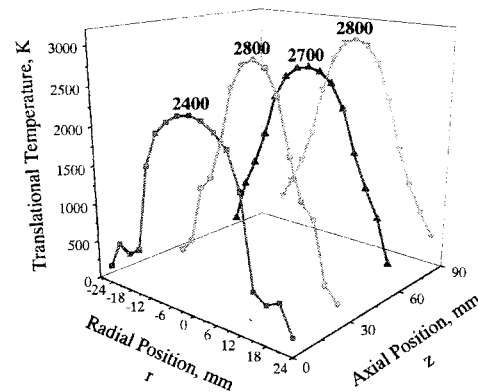
Fig.17 Translational temperature deducen from ArI in the argon-oxygen plume generated by University of Tokyo's arc-heater

7

Institute of Aeronautics and Astronautics